

## Magnetic and Electrocatalytic Properties of Transition Metal Doped MoS<sub>2</sub> Nanocrystals

L. M. Martinez<sup>1†</sup>, J. A. Delgado<sup>1†</sup>, C. L. Saiz<sup>1</sup>, A. Cosio<sup>1</sup>, Y. Wu<sup>2</sup>, D. Villagran<sup>2</sup>, K. Gandha<sup>3</sup>, C. Karthik<sup>4</sup>, I.C. Nlebedim<sup>3</sup>, S. R. Singamaneni<sup>1\*</sup>

<sup>1</sup>Department of Physics, The University of Texas at El Paso, El Paso, Texas 79968, USA

<sup>2</sup>Department of Chemistry, The University of Texas at El Paso, TX 79968, USA

<sup>3</sup>Critical Materials Institute, Ames Laboratory, Ames, Iowa 50011, USA

<sup>4</sup>Micron School of Materials Science and Engineering, Boise State University, 1910 University Drive, Boise, ID 83725, USA.

### Abstract

In this paper, the magnetic and electrocatalytic properties of hydrothermally grown transition metal doped (10% of Co, Ni, Fe and Mn) 2H-MoS<sub>2</sub> nanocrystals (NCs), with particle size 25-30 nm are reported. The pristine 2H-MoS<sub>2</sub> NCs showed a mixture of canted anti-ferromagnetic and ferromagnetic behavior. While Co, Ni, and Fe doped MoS<sub>2</sub> NCs revealed room temperature ferromagnetism, Mn doped MoS<sub>2</sub> NCs showed room temperature paramagnetism, predominantly. The ground state of all the materials is found to be canted-antiferromagnetic phase. To study electrocatalytic performance for hydrogen evolution reaction, polarization curves were measured for undoped and the doped MoS<sub>2</sub> NCs. At the overpotential of  $\eta = -300$  mV, the current densities, listed from greatest to least, are: FeMoS<sub>2</sub>, CoMoS<sub>2</sub>, MoS<sub>2</sub>, NiMoS<sub>2</sub>, and MnMoS<sub>2</sub>, and the order of catalytic activity found from Tafel slopes is: CoMoS<sub>2</sub> > MoS<sub>2</sub> > NiMoS<sub>2</sub> > FeMoS<sub>2</sub> > MnMoS<sub>2</sub>. The increasing number of catalytically active sites in Co doped MoS<sub>2</sub> NCs might be responsible for its superior electrocatalytic activity. The present results show that the magnetic order-disorder behavior and catalytic activity can be modulated by choosing the suitable dopants in NCs of 2D materials.

\*srao@utep.edu

† These authors contributed equally to this work

## Introduction

Two-dimensional (2D) transition metal dichalcogenides (TMDs) are a class of materials with the formula  $\text{MX}_2$ , where M is a transition metal element (Mo, W etc.) and X is a chalcogen (S, Se or Te). 2D TMDs form layered structures in the form X–M–X, with the chalcogen atoms in two hexagonal planes separated by a plane of metal atoms. The layer-dependent properties of nanoscale TMDs have recently attracted a great deal of attention due to their extraordinary electrocatalytic, biomedical and optoelectronic properties<sup>1-10</sup>. Unlike other 2D materials, such as graphene, these materials are semiconductors with tunable (1.3-1.8 eV) band gaps.

Recent observation<sup>11-13</sup> of intrinsic 2D ferromagnetism in monolayer van der Waals crystals such as  $\text{CrI}_3$ ,  $\text{Cr}_2\text{Ge}_2\text{Te}_6$ , and  $\text{VS}_2$  has invigorated the field of low-dimensional magnetism in layered compounds. The above 2D materials intrinsically contain magnetic elements such as Cr and V, which give rise to ferromagnetic behavior. In particular, there has been numerous theoretical works appeared<sup>14-30</sup> in realizing the dilute 2D semiconducting materials for next generation spintronic materials, which do not contain magnetic elements intrinsically, followed by promising experimental observations<sup>31-37</sup>. For instance, Yan and co-authors have shown<sup>32</sup> that up on Li intercalation, the crystal structure transformed from 2H to 1T phase, and the magnetism was significantly enhanced from diamagnetism to paramagnetism in 2H- $\text{MoS}_2$  nanostructures. With further annealing in argon atmosphere, the 2H phase recovered gradually from 1T phase, and the magnetism decreased correspondingly, attributed to the Mo atoms of 1T- $\text{MoS}_2$ . In another work<sup>31</sup>, freestanding  $\text{MoS}_2$  nanosheets reveal the clear room-temperature ferromagnetism for all the  $\text{MoS}_2$  nanosheets. Furthermore, results indicate that the saturation magnetizations of the nanosheets increase as the size decreases, attributed to the presence of edge spins on the edges of the nanosheets. Cao and co-authors have shown<sup>33</sup> vacancy induced ferromagnetism in  $\text{MoS}_2$

nanosheets. Huo and co-authors reported<sup>36</sup> that multilayer WS<sub>2</sub> nanosheets exhibit strong ferromagnetic behavior with saturation magnetization (M<sub>s</sub>) of 0.0058 emu/g and coercive field (H<sub>c</sub>) of 92 Oe at room temperature, attributed to the zigzag edge sulphur and tungsten atoms. In addition, few more reports have recently appeared<sup>34,35,37</sup> on the magnetic properties of TMD nanostructures up on doping with Co, and Mn prepared through hydrothermal method. However, to date, the experimental studies on the magnetic properties of TMD nanostructures are limited. Most of the prior works focused on the magnetic properties mainly at the low (<5-7%) doping level, and the relevance to their catalytic activity is not studied. To broaden the current knowledge and understanding on the doping induced magnetic and catalytic properties, a comprehensive experimental study is required –that forms the first part of this study.

TMD NCs are also known to show excellent catalytic properties<sup>38-44</sup>. For instance, MoS<sub>2</sub> is a potential hydrogen evolution material for clean energy applications. The evolution of hydrogen from water has allured the scientific community for the possibility of using hydrogen as a clean energy source. In the process of extracting hydrogen from water via HER, studies<sup>45-49</sup> have shown that Pt electrodes possess the best electrocatalytic properties. If it were not for the rarity of this element, the pursuit of other materials for the reaction would not be necessary. It is therefore in the best interest of the scientific community to find earth-abundant materials that can be used in place of Pt. One such earth-abundant material is MoS<sub>2</sub>, which, in its bulk form, has been suggested for use as a catalyst in the evolution of hydrogen. MoS<sub>2</sub> was originally studied as a catalyst for hydrodesulphurization<sup>50-53</sup>. It has been shown<sup>38-44</sup> that the electrocatalytic performance of MoS<sub>2</sub> can be improved when it is prepared in nanocrystalline form due to the formation of increasing number of active edge sites by doping with transition metals, in the same way as was done for

hydrodesulfurization. To study MoS<sub>2</sub> NCs as electrocatalysts for HER, MoS<sub>2</sub> NCs were doped with Fe, Ni, Co, and Mn. Then, the reaction kinetics, reaction mechanism, and charge transfer rates were examined.

Therefore, in this work, transition metal (Co, Ni, Fe, Mn) (10%) doped MoS<sub>2</sub> NCs were prepared and their magnetic and catalytic properties were studied. In particular, it has been shown that it is possible to induce room temperature weak ferromagnetism in Co, Ni and Fe doped MoS<sub>2</sub> NCs, while Mn doped MoS<sub>2</sub> NCs showed paramagnetic-like behavior at room temperature. Furthermore, the catalytic performance of doped materials is compared with respect to that of pure MoS<sub>2</sub> NCs. This study forms a significant step forward to introduce new opportunities for fully exploiting these materials for advanced spintronic and catalytic applications.

### **Experimental Details**

MoS<sub>2</sub> NCs were synthesized by using a most common facile, bottom-up ‘hydrothermal method’. Unlike other ‘top-down’ approaches (chemical exfoliation, sonication of bulk MoS<sub>2</sub>, electro-Fenton processing etc.) this route eliminates harsh synthesis conditions, excludes hazardous chemicals, and is faster. Hydrothermal method has been routinely employed<sup>35, 37, 54, 55</sup> in preparing the nanostructures of transition metal doped (Co, Cu, V, Mn) MoS<sub>2</sub> up to the doping level of 16%. Previously, this method was successfully employed<sup>56-58</sup> by some of us (Singamaneni, Gandha) in preparing nanocrystalline magnetic nanowires. To describe the procedure briefly, 0.4g of Na<sub>2</sub>MoO<sub>4</sub>·2H<sub>2</sub>O was dissolved in 30 ml distilled water under sonication for 20 minutes. At this step, the desired metal precursor is added. 0.38g of dibenzyl disulfide was then added to the solution along with 30mL of ethanol and sonicated for 30 minutes. The solution was then transferred into a 100 mL Teflon-lined stainless-steel autoclave and was maintained at 250 °C for

18 hrs. After 18 hrs. The reaction system was allowed to cool down to ambient temperature. The obtained products were collected by centrifugation and washed with deionized water. The stoichiometric MoS<sub>2</sub> NCs were filtered and left to dry over night at room temperature in vacuum. Using this approach, 10% Co, Ni, Fe and Mn doped MoS<sub>2</sub> NCs were prepared. All the precursors were purchased from Alfa Aesar without further purification. The magnetization measurements were performed using Quantum Design PPMS (5-300 K, ±5T). Electron spin resonance (ESR) data was recorded on a Bruker EMX Plus X-band (~9.40 GHz) ESR spectrometer, equipped with a high sensitivity probe head. A ColdEdge™ ER 4112HV In-Cavity Cryo-Free VT system connected with an Oxford temperature controller was used for low temperature measurements. The complete system was operated by Bruker Xenon software. Additionally, all ESR experimental settings were kept constant for reproducibility. For all ESR measurements, the sample was wrapped in Teflon tape, and inserted in quartz tube. During the magnetic measurements, all the samples were carefully handled with nonmagnetic capsules and tapes to avoid contamination. We have employed X-ray diffraction (XRD), transmission electron microscopy (TEM), Raman spectroscopy and X-ray photo absorption spectroscopy (XPS) measurements to study the crystallinity, phase formation, doping effects and valence states of elements before and after doping with transition metal elements (data not shown).

All catalysts were accessed heterogeneously for hydrogen production. Prior to electrochemical studies, the catalysts were deposited on a conductive fluorinated-tin oxide (FTO) substrate<sup>61</sup>, with a conductive adhesive silver paste to better support the catalyst. FTO glass was cleaned by being sonicated in acetone, isopropyl alcohol, and deionized water separately. Then the silver paste was coated on top of the active side of the FTO with an area of 0.25 cm<sup>2</sup> (0.5 cm \* 0.5 cm). 0.5 mg of

the catalyst was dispersed in 1 mL ethanol and sonicated for 30 minutes to form a homogeneous ink. 10  $\mu$ L of the catalyst ink was then drop casted on the silver paste and the plate was allowed to dry in ambience, which was later used as the working electrode for electrochemical measurements.

All electrochemical studies were performed on a CHI760D potentiostat<sup>61</sup> with a three-electrode electrochemical cell in room temperature. A platinum wire was utilized as the counter electrode while a saturated calomel electrode (SCE) was used as the reference electrode. All potentials displayed in this work were referred to reversible hydrogen electrode (RHE) by adding a value of  $(0.245 + 0.059 \text{ pH})$  to the data obtained using a SCE reference electrode. An aqueous solution of 0.5 M  $\text{H}_2\text{SO}_4$  was used as both the proton source and electrolyte. The solution was saturated with nitrogen gas to remove the dissolved oxygen prior to each measurement. Electrical impedance spectroscopy (EIS) was obtained at different overpotentials from 100 KHz to 0.1 Hz with AC voltage of 5 mV.

## **Results and Discussion**

### **A. Magnetic Properties**

#### **a. $\text{MoS}_2$ NCs**

To study the magnetic properties of  $\text{MoS}_2$  NCs, temperature- and magnetic field-dependent magnetization measurements were performed. In Fig. 1(a), the temperature dependence of

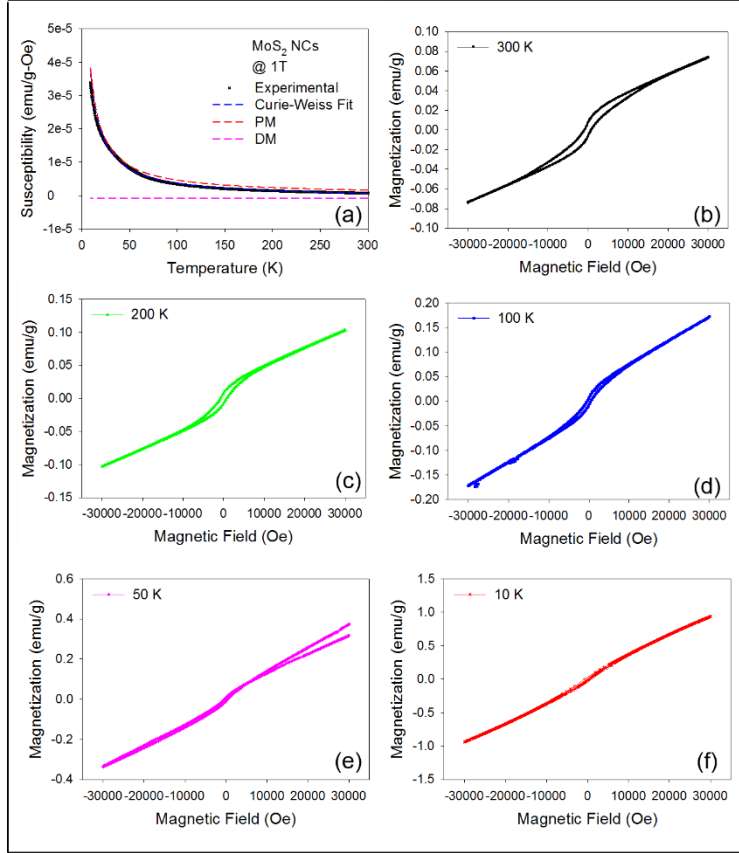


**Fig. 1:** The temperature dependent magnetic susceptibility and magnetic field-dependent magnetic behavior of MoS<sub>2</sub> NCs. Inset of Fig. 1(a) also included the applicability of modified Curie-Weiss model.

(CW) model<sup>32</sup>  $\chi = \chi_{dm} + C / (T + \theta)$ , which involves the diamagnetic and paramagnetic contributions. Here,  $\chi_{dm}$  is the diamagnetic susceptibility,  $C$  = Curie constant,  $\theta$  = CW temperature, and  $T$  = measurement temperature. The fitting results (blue) are shown in Fig. 1(a) along with the experimental data (black). Both the diamagnetic and paramagnetic components were resolved. In addition, the fitting results are tabulated in Table 1. The value of  $\theta$  was obtained as 3 K for the MoS<sub>2</sub> NCs. As shown in Table 1, the value of  $\theta$  is positive indicating antiferromagnetic behavior, which, however, is associated with uncompensated spins that result in finite magnetization. That is the typical signature of canted antiferromagnetic phase. Negative  $\theta$  values would indicate ferromagnetism.

magnetization is plotted. The magnetization was measured from 10-300 K, after a  $\mu_0H = 1$  T magnetic field cooling. As it can be noticed, the magnetization increased with cooling. A similar observation was reported on many other materials<sup>31,32,37,62</sup> such as exfoliated WS<sub>2</sub> nanosheets, graphene nanoribbons, Li intercalated MoS<sub>2</sub> nanosheets, and amorphous MoS<sub>2</sub>.

To better understand the observed magnetic behavior, the  $\chi$ -T curve was fitted using modified Curie-Weiss

Table 1

Sample	C	$\Theta$ (K)	$\chi_{dm}$
Undoped MoS <sub>2</sub> NCs	4.767e-04	3.406	-9.454e-07
Fe doped MoS <sub>2</sub> NCs	4.257e-04	3.296	-3.732e-07
Ni doped MoS <sub>2</sub> NCs	5.396e-04	3.173	-6.123e-07
Co doped MoS <sub>2</sub> NCs	9.895e-04	2.935	1.883e-06
Mn doped MoS <sub>2</sub> NCs	3.756e-03	2.841	-5.526e-06

Now, the attention will be turned to the magnetic field dependent magnetization behavior. Isothermal magnetization as a function of magnetic field were measured between 10-300 K. The data are plotted in Fig. 1(b-f). At 10 K, observation of a nearly anhysteretic behavior with positive slope indicates canted antiferromagnetic phase. As temperature increases further, a more magnetic hysteretic behavior was observed at low fields but the anhysteretic behavior persists at higher fields. These features together with M-T variation (Fig. 1(a)) indicate that MoS<sub>2</sub> NCs showed a canted antiferromagnetism at low temperature and weak ferromagnetism at room temperature. We have verified that the modified Brillouin function<sup>32</sup> (see below) could not account for the room temperature M-H behavior.

$$M = X_a H + M_s \left[ \frac{2J+1}{2J} \coth\left(\frac{2J+1}{2J} X\right) - \frac{1}{2J} \coth\left(\frac{X}{2J}\right) \right]$$

This function consists of a linearly field dependent function, which represents diamagnetism added with the classic Brillouin function, which refers to paramagnetism. In the above equation, the variable  $M_s$  is the saturated magnetization,  $M_s = Ng\mu J$ , where  $N$  is the density of spins,  $\mu$  is Bohr's magneton,  $g$  is the Lande  $g$ -factor, and  $J$  is the angular momentum number. The variable  $X$  is equaled to  $gJ\mu H/kT$ , where  $k$  is Boltzmann's constant, and  $T$  is temperature. By using the modified Brillouin function, we were able to obtain fits for the data that was accumulated, however the numerical values of temperature in our fits did not correlate with what was seen in

experimentation, verifying that the modified function could not account for the magnetic-field dependent magnetization data that was observed at room temperature. We noticed a strong hysteretic behavior at 300 K rather than at 10 K. This observation is also reflected in the temperature dependent coercive field ( $H_c$ ) trend plotted in Figure 2. We noticed that  $H_c$  increased from 373 to 880 Oe as the temperature increased from 10 to 300 K. This infers that the ferromagnetism observed at room temperature is of short-range.

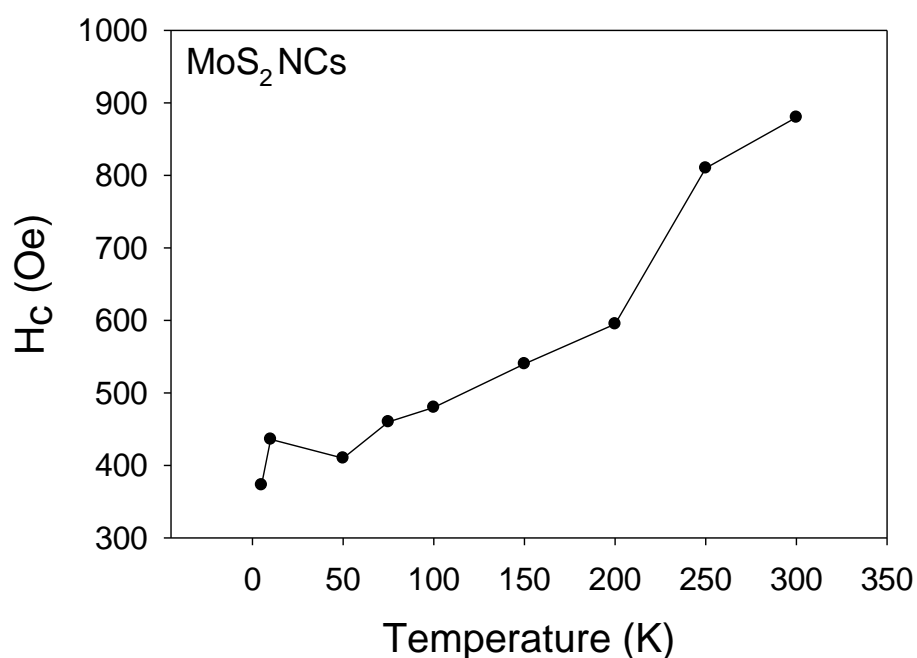


Figure 1: The temperature variation of coercive field of MoS<sub>2</sub> NCs

To corroborate the magnetic data, the temperature dependent (50-300 K) resistance measurements (data not shown) were performed on all the materials studied here, including undoped MoS<sub>2</sub> NCs. The data showed semiconducting behavior (resistance increases as the sample is cooled), consistent with the literature reports<sup>63</sup>, and revealed very little (<0.5%) magnetic field dependence even upon the application of 3 T magnetic field. These observations are the typical signatures of canted antiferromagnetism.

To provide additional information on the presence of magnetic moments, in our previous work<sup>59,60</sup>, using X-band (~9.43 GHz) ESR spectroscopy performed on MoS<sub>2</sub> NCs, we have reported several electron spin centers such as oxygen species, sulphur vacancies, thio-, and oxo-Mo<sup>5+</sup>. We believe that the exchange interaction among these magnetic species could lead to the observed magnetic phases. These measurements coupled with the data obtained from XPS and Raman spectroscopy showed no indication of unwanted extrinsic impurities that could account for the magnetic behavior observed in the present work.

In the sections below, the magnetic and catalytic properties of doped MoS<sub>2</sub> NCs were presented and discussed.

#### **b. Co doped MoS<sub>2</sub> NCs**

The temperature dependent magnetic susceptibility ( $\chi$ ) data was obtained after the sample was cooled to 10 K in  $\mu_0H = 1$  T magnetic field (see Fig. 3(a)). The magnetization value (0.8 emu/g) observed in the present study is higher than those (0.006 to 0.3 emu/g) reported<sup>35,37,54,55</sup> in the literature on similar systems such as Co, Cu, and V doped (< 7% doping) MoS<sub>2</sub> nanostructures prepared through hydrothermal method. As displayed in Fig. 3(a), the temperature dependence of magnetic susceptibility can be well described by the modified CW model. We obtained a positive  $\theta$  of 3 K (see Table 1) which indicates that the material is antiferromagnetic below the temperature of 3 K.

Isothermal magnetization measurements were performed on Co doped MoS<sub>2</sub> NCs by sweeping the magnetic field from -2 to +2 T at 10, 50, 100, 200 and 300 K. The data are presented in Fig. 3(b-e). At 10 K, magnetization shows anhysteretic behavior with the magnetic field with the positive

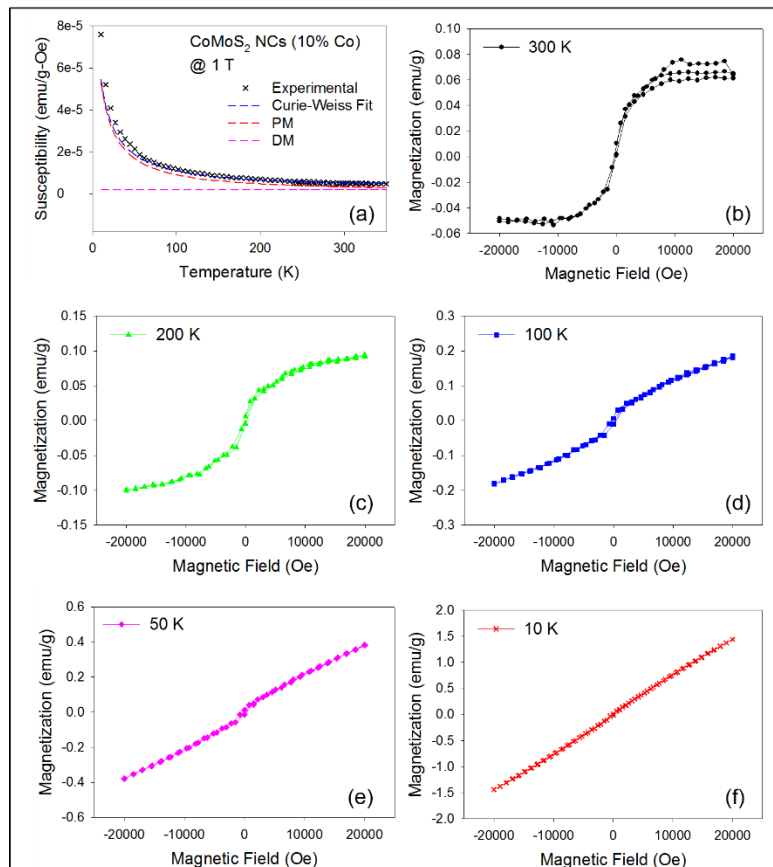


Figure II: The temperature dependent magnetic susceptibility and magnetic field-dependent magnetic behavior of Co doped (10%) MoS<sub>2</sub> NCs. Inset of Fig. 3(a) shows the applicability of modified Curie-Weiss model.

magnetization data observed at room temperature. The saturation magnetization (magnetization at the maximum applied magnetic field) decreases as the measurement temperature increases from 10-300 K. This trend is consistent with the temperature dependent magnetic susceptibility data as shown in Fig. 3(a). Xiang and co-authors have also reported<sup>35</sup> room temperature ferromagnetism from Co doped (< 7%) MoS<sub>2</sub> nanosheets.

XRD patterns (data not shown) obtained on the samples studied here are identical to the ones reported on the best samples prepared through hydrothermal method in the literature<sup>31,35,37,64</sup> thus confirming that there is no or minimal segregation/clustering of dopants. If there is a significant

slope, which indicates the (canted) antiferromagnetic behavior. Interestingly, with further increase in temperature, a more hysteretic behavior with coercive field of 400 Oe becomes pronounced, suggesting unambiguous room-temperature ferromagnetism, as evidenced from the s-shaped hysteresis loop. In addition, the applicability of the Brillouin function was tested, and found that

it could not be accounted for the magnetic-field dependent

clustering effect, one would expect to observe high ferromagnetic  $T_C$  much beyond room temperature<sup>65</sup>, which is clearly not the case here.

### c. Ni doped MoS<sub>2</sub> NCs

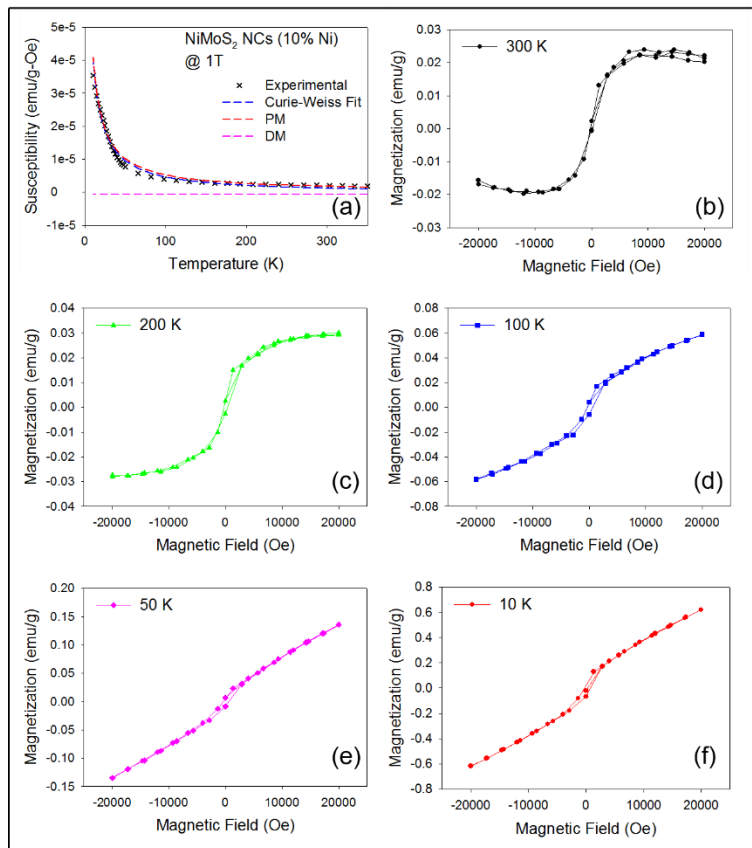


Figure III: The temperature dependent magnetic susceptibility and magnetic field-dependent magnetic behavior of Ni doped (10%) MoS<sub>2</sub> NCs. Inset of Fig. 4(a) shows the applicability of modified Curie-Weiss model.

Temperature dependent magnetic susceptibility data were collected after the sample was field cooled at  $\mu_0 H = 1$  T magnetic field (Fig. 4(a)). The magnetization value (0.4 emu/g) observed in the present study is comparable to those reported in the literature on similar systems<sup>35,37,54,55</sup>. The modified CW model, as depicted in Fig. 4(a) can describe the temperature dependent magnetization behavior. The obtained  $\theta$  is 3 K (see Table 1), which suggests that the material is antiferromagnetic below 3

K.

The isothermal magnetization measurements were performed on Ni doped MoS<sub>2</sub> NCs by sweeping the magnetic field from -2 to +2 T at 10, 50, 100, 200 and 300 K. The data are presented in Fig. 4(b-e). At 10 K, magnetization an hysteretic behavior as a function of magnetic field was observed, which indicates (canted) antiferromagnetic behavior. Interestingly, as temperature is increased

further, a hysteretic behavior with coercive field of 175 Oe appears, suggesting unambiguous room-temperature ferromagnetism. The saturation magnetization decreases as the measurement temperature increased from 10-300 K. This trend is consistent with the temperature dependent magnetic susceptibility data shown in Fig. 4(a). Similar to the case of Co doped MoS<sub>2</sub> NCs, Brillouin function could not account for the magnetic-field dependent magnetization data observed at room temperature. To our knowledge, with the exception of one report<sup>66</sup> on the catalytic behavior of Ni doped MoS<sub>2</sub> nanoparticles, there have been no previous works reported on the magnetic properties of Ni doped MoS<sub>2</sub> NCs, to compare our data at any doping percentage.

#### **d. Fe doped MoS<sub>2</sub> NCs**

Like the measurements performed on Co and Ni doped MoS<sub>2</sub> NCs, magnetization data were collected on Fe doped MoS<sub>2</sub> NCs. The temperature dependent magnetic susceptibility data was recorded after the sample was cooled in  $\mu_0H = 1$  T magnetic field (see Fig. 5(a)). The magnetization value (0.3 emu/g) obtained in the present study from  $\chi$ -T curve is comparable to that (0.25 emu/g) reported in the literature on 1.74% Fe doping in MoS<sub>2</sub> nanostructures<sup>64</sup>. As displayed in Fig. 5(a), it was found that the modified CW model describes well the temperature dependent magnetic susceptibility behavior. From the fits, the  $\theta$  is obtained as 3 K (see Table 1), which indicates that the material is antiferromagnetic below 3 K.

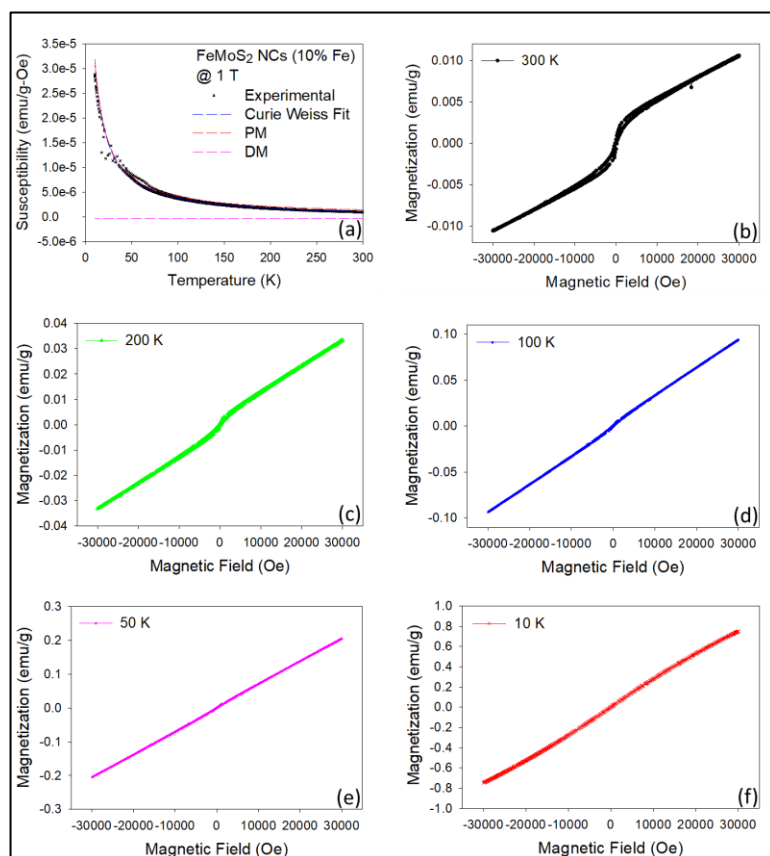


Figure IV: The temperature dependent magnetic susceptibility and magnetic field-dependent magnetic behavior of Fe doped (10%) MoS<sub>2</sub> NCs. Inset of Fig. 5(a) shows the applicability of modified Curie-Weiss model.

The isothermal magnetization data is presented in Fig. 5(b-e). At 10 K, similar to the previous samples, magnetization shows anhysteretic behavior with the magnetic field, which indicates (canted) antiferromagnetic behavior. However, at 300 K, the M-H behavior of this material shows a combination of ferromagnetic (at low fields) and antiferromagnetic behavior (at high fields). This is in sharp contrast with the Co and Ni doped samples, which show complete ferromagnetic behavior at room temperature. The saturation magnetization decreases as the measurement temperature increased from 10-300 K. This trend is consistent with the temperature dependent magnetic susceptibility data shown in Fig. 5(a). In addition, it has been verified that Brillouin function could not account for the magnetic-field dependent magnetization data observed at 300 K. Xia and co-authors also reported<sup>64</sup> room temperature ferromagnetism in Fe doped (<3.18%) MoS<sub>2</sub> nanosheets prepared through hydrothermal process. The interaction between the sulfur vacancies and the dopants is argued to be at play. A similar situation may be expected to happen in the present case as well.

The isothermal magnetization data is presented in Fig. 5(b-e). At 10 K, similar to the previous samples, magnetization shows anhysteretic behavior with the magnetic field, which indicates (canted) antiferromagnetic behavior. However, at 300 K, the M-H behavior of this material shows a combination of ferromagnetic (at low fields) and antiferromagnetic behavior (at high fields). This is in sharp contrast with the Co and Ni doped samples, which show

### e. Mn doped MoS<sub>2</sub> NCs

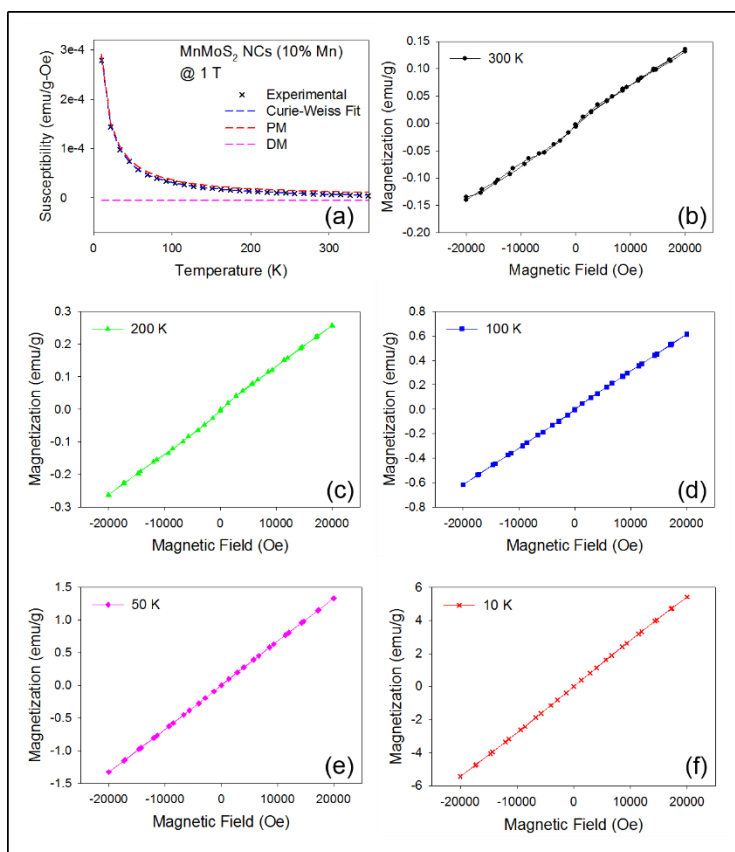


Figure V: The temperature dependent magnetic susceptibility and magnetic field-dependent magnetic behavior of Mn doped (10%) MoS<sub>2</sub> NCs. Inset of Fig. 6(a) shows the applicability of modified Curie-Weiss model.

insights into the magnetism,  $\chi$ -T curve was fitted to the modified CW model comprising both diamagnetic and paramagnetic contributions. The highest Curie's constant of  $4 \times 10^{-3}$  obtained from the  $\chi$ -T curve fitting signifies the larger magnetization in comparison to the materials discussed above. The fitting results are shown in Fig. 6(a) along with the experimental data. Using this model, the diamagnetic and paramagnetic components were resolved and obtained CW constant ( $\theta$ ) as 3 K (see Table 1), which indicates that the material is antiferromagnetic below 3 K. However, a much weaker ferromagnetism was observed at 300 K as reflected from the hysteretic behavior

Temperature dependent magnetic susceptibility and magnetic field dependent magnetization measurements were performed on Mn doped MoS<sub>2</sub> NCs. As shown in Fig. 6(a), the magnetic susceptibility increased as the sample temperature is lowered from 300 K to 10 K. More importantly, it was noticed that the magnetization (measured at 10 K, 1T) is about 6-times higher than that of pure MoS<sub>2</sub> NCs (see Fig. 1(a)). This observation is the direct effect of doping with Mn. To gain additional

at low fields, and a predominant paramagnetic nature was observed at higher fields. A similar weak ferromagnetism was previously reported<sup>67</sup> for Mn doped SnSe alloys prepared via molecular beam epitaxy methods. Wang and co-workers reported<sup>37</sup> room temperature ferromagnetism in Mn doped (7%) MoS<sub>2</sub> NCs. Park and co-authors have reported<sup>68</sup> a similar room temperature ferromagnetism from MoS<sub>2</sub> NCs upon doping with MnO<sub>2</sub> by electrochemical method, associated with the saturation magnetization of 0.02emu/g. This work not only shows that magnetic properties strongly depend on the nature of the dopant but also the magnetic order-disorder transition varies with dopant type such that Co and Ni doping produces stronger ferromagnetic behavior than Fe and Mn at least at 300 K.

Now, the catalytic properties of these materials are discussed below.

## **B. Electrocatalytic Properties**

It has been shown that the electrocatalytic performance of MoS<sub>2</sub> NCs can be engineered by doping the active edge sites with transition metals. To study HER performance, polarization curves (see Fig. 7) were obtained for MoS<sub>2</sub> NCs and the doped samples. At an overpotential ( $\eta$ ) of 300 mV, the current densities for MoS<sub>2</sub>, CoMoS<sub>2</sub>, NiMoS<sub>2</sub>, FeMoS<sub>2</sub> and MnMoS<sub>2</sub> were found to be 2.09, 3.00, 1.5, 4.05 mA/cm<sup>2</sup> and 52 uA/cm<sup>2</sup>. Listed from greatest to least for comparison, the reaction kinetics are as follows: FeMoS<sub>2</sub> > CoMoS<sub>2</sub> > MoS<sub>2</sub> > NiMoS<sub>2</sub> > MnMoS<sub>2</sub>; this was observed to be true for  $-372.8 \text{ mV} \leq \eta \leq -169.6 \text{ mV}$ . This progression is the exact same order of activity that was previously found by calculating the hydrogen absorption free energy ( $\Delta G_H$ ). H. Wang et al. and other groups have doped different transition metals to MoS<sub>2</sub> nanostructures similar to the metals we used and observed current densities that are comparable with our data<sup>69-71</sup>. The onset potential for our MoS<sub>2</sub> NCs was 141 mV; this is comparable to the work done by X. Ren<sup>72</sup>. Thus,

the present observations are consistent with the literature reports.

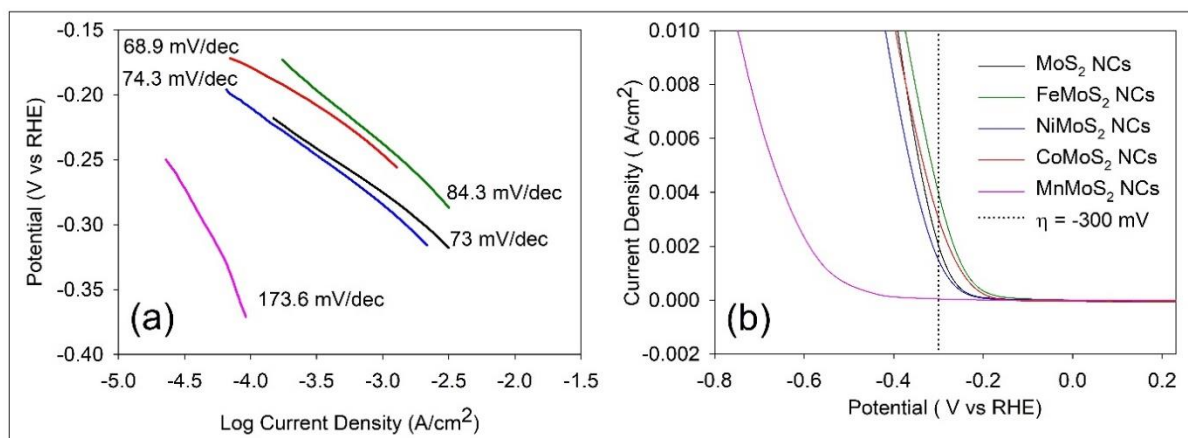


Figure VI: (a) Polarization curves, (b) Tafel plots of pristine and 10% doped (Co, Ni, Fe, and Mn) MoS<sub>2</sub> NCs.

For the HER, the Tafel slope and exchange current density can provide information about the reaction mechanism and kinetics of the process. The Tafel slopes also indicate the rate-limiting step in the HER<sup>73</sup>. Essentially, the lower the Tafel slope, the faster the reaction takes place, and the faster hydrogen is produced. Doping with different transition metals showed a slight change in the Tafel slope, which is consistent with other literature reports<sup>69, 70, 74, 75</sup>.

EIS was performed on the samples at overpotentials of 0.445, 0.5, 0.545, and 0.645 V. Figure 8 shows the EIS measurements taken at  $\eta = 0.5$  V. Smaller semicircle diameters correspond to higher charge transfer, higher conductivity, and thus lower charge transfer resistance ( $R_{ct}$ ). The samples can be ranked in order from least to greatest  $R_{ct}$  in the following order: Fe, Co, pristine MoS<sub>2</sub>, Ni, Mn. Fe doped MoS<sub>2</sub> NCs have the greatest conductivity and charge transfer ability, while Mn-doped MoS<sub>2</sub> NCs have the least. Another literature report performed a similar electrocatalytic study of TM-doped MoS<sub>2</sub> and found the exact same progression<sup>69</sup>, with  $R_{ct}$  increasing from Fe to Ni in the same order. This study (Figure 8 (b)) of Mn doped MoS<sub>2</sub> showed poor HER performance.

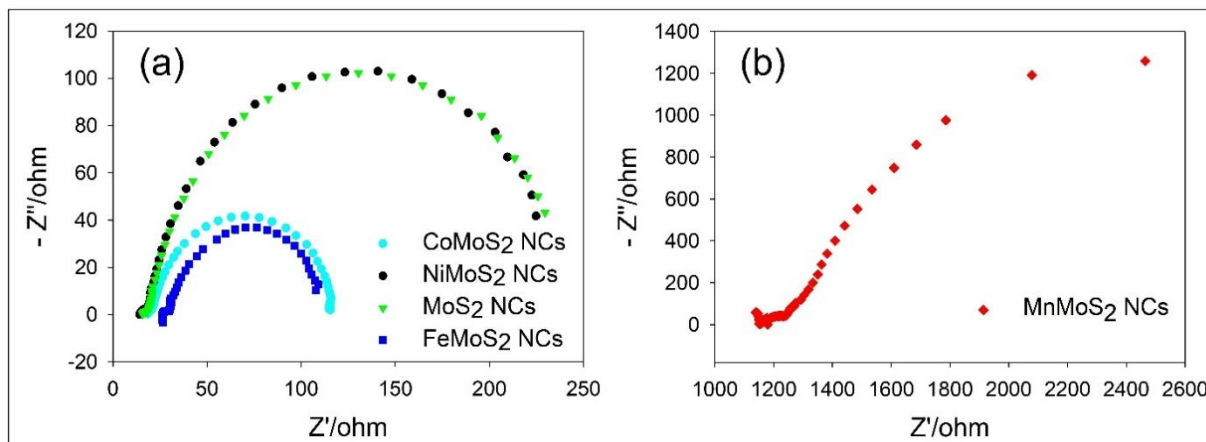


Figure VII: (a) EIS plots for Co, Ni, Fe doped MoS<sub>2</sub> NCs, and pristine MoS<sub>2</sub> NCs;  $\eta = 0.5V$ . (b) EIS plot for Mn doped MoS<sub>2</sub> NCs;  $\eta = 0.5V$ .

The electrocatalytic performance of CoMoS<sub>2</sub> NCs was examined using chronoamperometry to determine the long-term stability of the NCs. The chronoamperometric studies were operated in a custom-built two-compartment gas-tight electrochemical cell under an argon atmosphere. One of the compartment of the cell contains the working electrode and the reference electrode while the other compartment contains the counter electrode. The solution (0.5 M H<sub>2</sub>SO<sub>4</sub> in water) was saturated with argon gas prior to the measurement and the solution in the side of the cell containing the working electrode was kept stirring to remove the in-situ generated hydrogen gas. The experiment was conducted with an initial current density of 10 mA/cm<sup>2</sup> along with a constant overpotential of  $\eta=850$  mV. The current density was observed to stabilize after approximately 5 hours, and after over 23 hours of operation, the CoMoS<sub>2</sub> NC's can be seen to be electrocatalytically active. Thus, the stability of the nanocrystals has been demonstrated through pragmatic means.

Interestingly, the electrochemical behavior shown in this work is in agreement with what is known in the literature<sup>69,76,77</sup>. The electrocatalytic activity is  $\text{FeMoS}_2 > \text{CoMoS}_2 > \text{MoS}_2 > \text{NiMoS}_2 > \text{MnMoS}_2$  consistent with previous works<sup>69,76,77</sup>. Since the adsorbed atomic hydrogen Gibbs free energy ( $\Delta G_H$ ) is the key to the HER electrocatalytic activity of a catalyst,  $\Delta G_H$  closer to zero corresponds to higher activity. Incorporation of transition metals to  $\text{MoS}_2$  does not affect the  $\Delta G_H$  of the Mo-edge but lowers the  $\Delta G_H$  of S-edge, which makes the catalytic inert S-edge catalytic, active. Previous studies<sup>69,76,77</sup> have shown similar effects when doping with Fe and Co leading to  $\Delta G_H$  value closer to zero in the S-edge of  $\text{MoS}_2$ , which explains why these two catalysts exhibit the best efficiency.

Now, why the variations in the magnetic and catalytic properties of the studied materials occur as a function of transition metal doping is discussed. The present work as well as the early-on reports<sup>78-81</sup> showed that the transition metal elements show interesting magnetic properties as well as pronounced catalytic activity. From our experimental observations, we learned that the Mn doped  $\text{MoS}_2$  NCs showed least catalytic performance and showed predominant paramagnetism at room temperature. Whereas the pristine  $\text{MoS}_2$  and Co, Ni, and Fe doped  $\text{MoS}_2$  NCs showed good catalytic performance as well as stronger room temperature ferromagnetism. To better understand the relationship between the magnetism and catalytic performance, X-band ESR measurements were performed on all the samples at room temperature (300 K). The data is plotted in Figure 9. As it can be clearly noticed, Mn doped  $\text{MoS}_2$  NCs did not show signals coming from the catalytically active centers, except the strong signal that comes from  $\text{Mn}^{2+}$  only. On the other hand, the samples doped with Co, and Ni including undoped  $\text{MoS}_2$  NCs showed many sharp ESR signals, indicating the presence of larger number of catalytically active centers. Hence, we believe that Co doped  $\text{MoS}_2$  NCs showed superior catalytic performance compared to Mn doped  $\text{MoS}_2$  NCs. These

active defect centers contain unpaired electron spins due to uncoordinated and dangling bonds. The observed ferromagnetic behavior could have resulted from the interaction between these active spin centers.

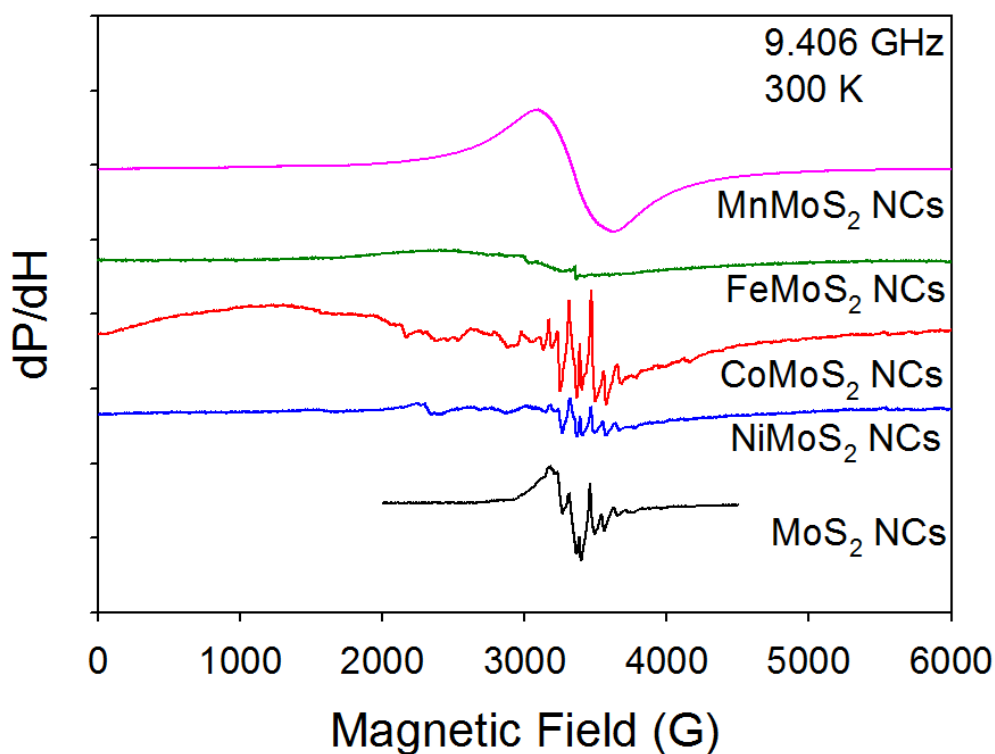


Figure VIII: X-band room temperature (300 K) ESR spectra collected from MoS<sub>2</sub>, Co, Ni, Fe, and Mn doped MoS<sub>2</sub> NCs

Furthermore, the morphology of 10% Co doped MoS<sub>2</sub> NCs is distinctly different from that of 10% Mn doped MoS<sub>2</sub> NCs, as reflected from the TEM bright field images displayed in Fig.10. The Co doped sample shows a flowery morphology with randomly oriented sheets of MoS<sub>2</sub> that are only a few monolayers thick as indicated by the SAED pattern shown as inset. On the other hand, the Mn doped MoS<sub>2</sub> showed a mixed morphology with some flowery structures, but also mixed with many faceted plates of well crystallized shaped MoS<sub>2</sub> that are several hundred nanometers wide

and the corresponding SAED pattern is shown as inset. The [111] zone axis SAED pattern indicates single crystalline nature of these plates with six fold symmetry. One would expect the flowery shaped morphology of Co doped samples to have more surface area compared to the Mn doped samples, which would explain the high catalytic activity of these samples.

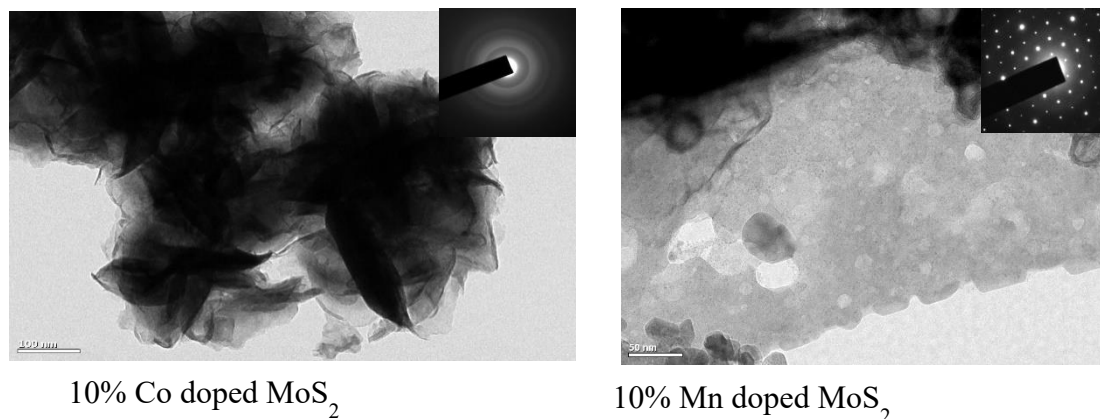


Fig. x: Bright field transmission electron microscopic image of 10% Co doped MoS<sub>2</sub> (left) and 10% Mn doped MoS<sub>2</sub> nanocrystals (right)

## Conclusions

To conclude, the magnetic and catalytic properties of hydrothermally grown transition metal doped (10% of Co, Ni, Fe and Mn) MoS<sub>2</sub> NCs associated with the particle size of 25-30 nm have been reported. Interestingly, the undoped MoS<sub>2</sub> NCs showed a mixture of canted anti-ferromagnetic and ferromagnetic behavior. MoS<sub>2</sub> NCs doped with Co, Ni, and Fe exhibited profound room temperature ferromagnetism. On the other hand, Mn doped MoS<sub>2</sub> NCs showed room temperature paramagnetic nature, predominantly. For all the materials, modified CW law described the temperature dependent magnetic behavior, and the ground state is canted antiferromagnetic phase associated with uncompensated electron spins. In addition, the hydrogen evolution reaction performance was also studied. The present study compared the current densities ( $j$ ), measured at

the overpotential of  $-372.8 \text{ mV} \leq \eta \leq -169.6 \text{ mV}$ , listed from greatest to least,  $j(\text{FeMoS}_2) = 4.05$ ,  $j(\text{CoMoS}_2) = 3.00$ ,  $j(\text{MoS}_2) = 2.09$ ,  $j(\text{NiMoS}_2) = 1.5 \text{ mA/cm}^2$ , and  $j(\text{MnMoS}_2) = 52 \text{ uA/cm}^2$ . The order of overall reaction activity is obtained from Tafel slopes as  $\text{CoMoS}_2 > \text{MoS}_2 > \text{NiMoS}_2 > \text{FeMoS}_2 > \text{MnMoS}_2$ . The electrochemical impedance spectroscopic measurements indicated that Fe doped  $\text{MoS}_2$  NCs have the best conductivity and charge transfer ability, while Mn-doped  $\text{MoS}_2$  had the lowest. Co doped  $\text{MoS}_2$  NCs show best catalytic activity when compared to Mn doped  $\text{MoS}_2$  NCs. Most likely, it is due to the creation of more number of catalytically active centers in Co doped  $\text{MoS}_2$  NCs compared to Mn doped  $\text{MoS}_2$  NCs as evidenced from room temperature ESR measurements.

### **Acknowledgements**

L.M.M, J.A.D, C. L.S, A. C, and S.R.S acknowledge support from a UTEP start-up grant. L.M.M acknowledges the Wiemer Family for awarding Student Endowment for Excellence. S.R.S acknowledges the NSF-PREM program (DMR – 1205302). Work at Ames Laboratory by I.C.N and K.G was supported by the Critical Materials Institute, an Energy Innovation Hub funded by the U.S. Department of Energy, Office of Energy Efficiency and Renewable Energy, Advanced Manufacturing Office. Work at Ames Laboratory, operated by Iowa State University, was performed under Contract No. DE-AC02-07CH11358.

## References

- [1]. Q. H. Wang, K. K-Zadeh, A. Kis, J. N. Coleman, and M. S. Strano, Electronics and optoelectronics of two-dimensional transition metal dichalcogenides, *Nature Nanotechnology* **7**, 699 (2012).
- [2]. G. R. Bhimanapati, Z. Lin et al., Recent Advances in Two-Dimensional Materials beyond Graphene, *ACS Nano* **12**, 11509 (2015).
- [3]. S. Z. Butler, S. M. Hollen et al., Progress, Challenges, and Opportunities in Two-Dimensional Materials Beyond Graphene, *ACS Nano* **12**, 2898 (2013).
- [4]. Zhong Lin, Bruno RCarvalho, Ethan Kahn, Ruitao Lv, Rahul Rao, Humberto Terrones, MarcosAPimenta and Mauricio Terrones, Defect engineering of two-dimensional transition metal Dichalcogenides, *2D Mater.* **3**, 022002 (2016).
- [5]. Haider I. Rasool, Colin Ophus, and Alex Zettl, Atomic Defects in Two Dimensional Materials, *Adv. Mater.* **27**, 5771 (2015).
- [6]. Jinhua Hong, Zhixin Hu, Matt Probert, Kun Li, Danhui Lv, Xinan Yang, Lin Gu, Nannan Mao, Qingliang Feng, Liming Xie, Jin Zhang, Dianzhong Wu, Zhiyong Zhang, Chuanhong Jin, Wei Ji, Xixiang Zhang, Jun Yuan & Ze Zhang, Exploring atomic defects in molybdenum disulphide monolayers, 6:6293 | DOI: 10.1038/ncomms7293
- [7]. Amin Azizi, Xiaolong Zou, Peter Ercius, Zhuhua Zhang, Ana Laura Eli'as, Ne'stor Perea-Lo'pez, Greg Stone, Mauricio Terrones, Boris I. Yakobson & Nasim Alem, Dislocation motion and grain boundary migration in two-dimensional tungsten disulphide, *Nature Communications* **5**, 4867 (2014).
- [8]. Xiao-Xi Li, Zhi-Qiang Fan, Pei-Zhi Liu, Mao-Lin Chen, Xin Liu, Chuan-Kun Jia, Dong-Ming Sun, Xiang-Wei Jiang, Zheng Han, Vincent Bouchiat, Jun-Jie Guo, Jian-Hao Chen & Zhi-Dong Zhang, Gate-controlled reversible rectifying behaviour in tunnel contacted atomically-thin MoS<sub>2</sub> transistor, *Nature Communications*, |DOI: 10.1038/s41467-017-01128-9.
- [9]. Rajendra Kurapati, Kostas Kostarelos, Maurizio Prato, and Alberto Bianco, Biomedical Uses for 2D Materials Beyond Graphene: Current Advances and Challenges Ahead, *Adv. Mater.*, **28**, 6052 (2016).
- [10]. Yinghui Sun, Rongming Wang, and Kai Liu, Substrate induced changes in atomically thin 2-dimensional semiconductors: Fundamentals, engineering, and applications, *APPLIED PHYSICS REVIEWS* **4**, 011301 (2017)
- [11]. Bevin Huang, Genevieve Clark, Efrén Navarro-Moratalla, Dahlia R. Klein, Ran Cheng, Kyle L. Seyler, Ding Zhong, Emma Schmidgall, Michael A. McGuire, David H. Cobden, Wang Yao, Di Xiao, Pablo Jarillo-Herrero & Xiaodong Xu, Layer-dependent ferromagnetism in a van der Waals crystal down to the monolayer limit, *Nature* **546**, 271 (2017).

- [12]. Cheng Gong, Lin Li, Zhenglu Li, Huiwen Ji, Alex Stern, Yang Xia, Ting Cao, Wei Bao, Chenzhe Wang, Yuan Wang, Z. Q. Qiu, R. J. Cava, Steven G. Louie, Jing Xia & Xiang Zhang, Discovery of intrinsic ferromagnetism in two-dimensional van der Waals crystals, *Nature*, **546**, 265 (2017).
- [13]. Manuel Bonilla, Sadhu Kolekar, Yujing Ma, Horacio Coy Diaz, Vijaysankar Kalappattil, Raja Das, Tatiana Eggers, Humberto R. Gutierrez, Manh-Huong Phan and Matthias Batzill, Strong room-temperature ferromagnetism in VSe<sub>2</sub> monolayers on van der Waals substrates, *Nature Nanotechnology* (2018), DOI.org/10.1038/s41565-018-0063-9.
- [14]. Rohan Mishra, Wu Zhou, Stephen J. Pennycook, Sokrates T. Pantelides, and Juan-Carlos Idrobo, Long-range ferromagnetic ordering in manganese-doped two-dimensional dichalcogenides, *Phys. Rev. B* **88**, 144409 (2013).
- [15]. Ramasubramaniam, A.; Naveh, D. Mn-Doped Monolayer MoS<sub>2</sub>: An Atomically Thin Dilute Magnetic Semiconductor, *Phys. Rev. B: Condens. Matter Mater. Phys.*, **87**, 195201 (2013), DOI: 10.1103/PhysRevB.87.195201.
- [16]. Y. C. Cheng,<sup>1</sup> Z. Y. Zhu,<sup>1</sup> W. B. Mi,<sup>2</sup> Z. B. Guo, and U. Schwingenschlogl, Prediction of two-dimensional diluted magnetic semiconductors: Doped monolayer MoS<sub>2</sub> systems, *Phys. Rev. B* **87**, 100401(R) (2013)
- [17]. Zhuhua Zhang, Xiaolong Zou, Vincent H. Crespi, and Boris I. Yakobson, Intrinsic Magnetism of Grain Boundaries in Two-Dimensional Metal Dichalcogenides, *ACS Nano* **7**, 10475 (2013).
- [18]. Oleg V. Yazyev and Yong P. Chen, Polycrystalline graphene and other two-dimensional materials, *NATURE NANOTECHNOLOGY*, **9**, 755 (2014).
- [19]. Yongqing Cai, Hangbo Zhou, Gang Zhang, and Yong-Wei Zhang, Modulating Carrier Density and Transport Properties of MoS<sub>2</sub> by Organic Molecular Doping and Defect Engineering, *Chem. Mater.*, **28**, 8611 (2016).
- [20]. Aleksandra Vojvodic, Berit Hinnemann, and Jens K. Nørskov, Magnetic edge states in MoS<sub>2</sub> characterized using density-functional theory, *Phys. Rev. B* **80**, 125416 (2009).
- [21]. Antonis N. Andriotis, Madhu Menon, Tunable magnetic properties of transition metal doped MoS<sub>2</sub>, *Phys. Rev. B* **90**, 125304 (2014).
- [22]. Qu Yue, Zhengzheng Shao, Shengli Chang and Jingbo Li, Adsorption of gas molecules on monolayer MoS<sub>2</sub> and effect of applied electric field, *Nanoscale Research Letters*, **8**, 425 (2013).
- [23]. Yafei Li, Zhen Zhou, Shengbai Zhang, and Zhongfang Chen, MoS<sub>2</sub> Nanoribbons: High Stability and Unusual Electronic and Magnetic Properties, *J. AM. CHEM. SOC.*, **130**, 16739 (2008).

- [24]. MPK Sahoo, Jie Wang, Yajun Zhang, Takahiro Shimada, and Takayuki Kitamura, Modulation of Gas Adsorption and Magnetic Properties of Monolayer-MoS<sub>2</sub> by Antisite Defect and Strain, *J. Phys. Chem. C*, **120**, 14113 (2016).
- [25]. Jiangang He, Kechen Wu, Rongjian Sa, Qiaohong Li, and Yongqin Wei, Magnetic properties of nonmetal atoms absorbed monolayers, *Appl. Phys. Lett.*, **96**, 082504 (2010)
- [26]. Min Kan, Subash Adhikari and Qiang Sun, Ferromagnetism in MnX<sub>2</sub> (X = S, Se) monolayers, *Phys.Chem.Chem.Phys.*, **16**, 4990 (2014).
- [27]. Xianqing Lin and Jun Ni, Charge and magnetic states of Mn-, Fe-, and Co-doped monolayer MoS<sub>2</sub>, *J. Appl. Phys.* **116**, 044311 (2014)
- [28]. Shang-Chun Lu and Jean-Pierre Leburton, Electronic structures of defects and magnetic impurities in MoS<sub>2</sub> monolayers, *Nanoscale Research Letters*, **9**, 676 (2014).
- [29]. Aleksander A. Tedstone, David J. Lewis, and Paul O'Brien, Synthesis, Properties, and Applications of Transition Metal-Doped Layered Transition Metal Dichalcogenides, *Chem. Mater.* **28**, 1965 (2016).
- [30]. Wun-Fan Li, Changming Fang, and Marijn A. van Huis, Strong spin-orbit splitting and magnetism of point defect states in monolayer WS<sub>2</sub>, *Phys. Rev. B* **94**, 195425 (2016).
- [31]. Daqiang Gao, Mingsu Si, Jinyun Li, Jing Zhang, Zhipeng Zhang, Zhaolong Yang and Desheng Xue, Ferromagnetism in freestanding MoS<sub>2</sub> nanosheets, *Nanoscale Research Letters*, **8**, 129 (2013).
- [32]. Shiming Yan, Wen Qiao, Xueming He, Xiaobing Guo, Li Xi, Wei Zhong, and Youwei Du, Enhancement of magnetism by structural phase transition in MoS<sub>2</sub>, *Appl. Phys. Lett.*, **106**, 012408 (2015).
- [33]. Liang Cai, Jingfu He, Qinghua Liu, Tao Yao, Lin Chen, Wensheng Yan, Fengchun Hu, Yong Jiang, Yidong Zhao, Tiandou Hu, Zhihu Sun, and Shiqiang Wei, Vacancy-Induced Ferromagnetism of MoS<sub>2</sub> Nanosheets, *J. Am. Chem. Soc.*, **137**, 2622 (2015).
- [34]. Kehao Zhang, Simin Feng, Junjie Wang, Angelica Azcatl, Ning Lu, Rafik Addou, Nan Wang, Chanjing Zhou, Jordan Lerach, Vincent Bojan, Moon J. Kim, Long-Qing Chen, Robert M. Wallace, Mauricio Terrones, Jun Zhu, and Joshua A. Robinson, Manganese Doping of Monolayer MoS<sub>2</sub>: The Substrate Is Critical, *Nano Lett.*, **15**, 6586 (2015).
- [35]. Zhong Cheng Xiang, Zhong Zhang, XiJin Xu, Qin Zhang, QingBao Wang and Chengwu Yuan, Room-temperature ferromagnetism in Co doped MoS<sub>2</sub> sheets, *Phys. Chem. Chem. Phys.*, **17**, 15822 (2015).
- [36]. Nengjie Huo, Yan Li, Jun Kang, Renxiong Li, Qinglin Xia, and Jingbo Li, Edge-states ferromagnetism of WS<sub>2</sub> nanosheets, *Appl. Phys. Lett.*, **104**, 202406 (2014).

- [37]. Jieqiong Wang, Fan Sun, Sen Yang, Yitong Li, Chuan Zhao, Minwei Xu, Yin Zhang, and Hao Zeng, Robust ferromagnetism in Mn-doped MoS<sub>2</sub> nanostructures, *Appl. Phys. Lett.*, **109**, 092401 (2016).
- [38]. Yifei Yu, Sheng-Yang Huang, Yanpeng Li, Stephan N. Steinmann, Weitao Yang, and Linyou Cao, Layer-Dependent Electrocatalysis of MoS<sub>2</sub> for Hydrogen Evolution, *Nano Lett.*, **14**, 553 (2014).
- [39]. Rui Peng, Liangbo Liang, Zachary D. Hood, Abdelaziz Boulesbaa, Alexander Poretzky, Anton V. Ievlev, Jeremy Come, Olga S. Ovchinnikova, Hui Wang, Cheng Ma, Miaofang Chi, Bobby G. Sumpter, and Zili Wu, In-Plane Heterojunctions Enable Multiphasic Two-Dimensional (2D) MoS<sub>2</sub> Nanosheets As Efficient Photocatalysts for Hydrogen Evolution from Water Reduction, *ACS Catal.*, **6**, 6723 (2016).
- [40]. Thomas F. Jaramillo, Kristina P. Jørgensen, Jacob Bonde, Jane H. Nielsen, Sebastian Horch, Ib Chorkendorff, Identification of Active Edge Sites for Electrochemical H<sub>2</sub> Evolution from MoS<sub>2</sub> Nanocatalysts, *SCIENCE*, **317**, 100 (2007)
- [41]. Yuzi Xu, Longlu Wang, Xia Liu, Shuqu Zhang, Chengbin Liu, Dafeng Yan, Yunxiong Zeng, Yong Pei, Yutang Liuc and Shenglian Luo, Monolayer MoS<sub>2</sub> with S vacancies from interlayer spacing expanded counterparts for highly efficient electrochemical hydrogen production, *J. Mater. Chem. A*, **4**, 16524 (2016).
- [42]. Ying Yin, Jiecai Han, Yumin Zhang, Xinghong Zhang, Ping Xu, Quan Yuan, Leith Samad, Xianjie Wang, Yi Wang, Zhihua Zhang, Peng Zhang, Xingzhong Cao, Bo Song, and Song Jin, Contributions of Phase, Sulfur Vacancies, and Edges to the Hydrogen Evolution Reaction Catalytic Activity of Porous Molybdenum Disulfide Nanosheets, *J. Am. Chem. Soc.*, **138**, 7965 (2016).
- [43]. Xiaoping Dai, Kangli Du, Zhazhao Li, Mengzhao Liu, Yangde Ma, Hui Sun, Xin Zhang, and Ying Yang, Co-Doped MoS<sub>2</sub> Nanosheets with the Dominant CoMoS Phase Coated on Carbon as an Excellent Electrocatalyst for Hydrogen Evolution, *ACS Appl. Mater. Interfaces*, **7**, 27242 (2015).
- [44]. Guoliang Liu, Alex W. Robertson, Molly Meng-Jung Li, Winson C. H. Kuo, Matthew T. Darby, Mohamad H. Muhieddine, Yung-Chang Lin, Kazu Suenaga, Michail Stamatakis, Jamie H. Warner, and Shik Chi Edman Tsang, MoS<sub>2</sub> monolayer catalyst doped with isolated Co atoms for the hydrodeoxygenation reaction, *Nature Chemistry*, DOI: 10.1038/NCHEM.2740 (2017).
- [45] Appleby, A. J. *Electrocatalysis and fuel cells. Catal. Rev.* **4**, 221–244 (1970)
- [46] Kinoshita, K. *Electrochemical Oxygen Technology* (Wiley, New York, 1992).
- [47] Toda, T., Igarashi, H., Uchida, H. & Watanabe, M. Enhancement of the electroreduction of oxygen on Pt alloys with Fe, Ni and Co. *J. Electrochem. Soc.* **146**, 3750–3756 (1999).

- [48] Markovic, N. M., Radmilovic, V. & Ross, P. N. in *Catalysis and Electrocatalysis at Nanoparticle Surfaces* (eds Wieckowski, A., Savinova, E. & Vayenas, C.) Ch. 9 (Marcel Dekker, New York, Basel, 2003).
- [49] Mukerjee, S. & Srinivasan, S. Enhanced electrocatalysis of oxygen reduction reaction on platinum alloys in proton-exchange membrane fuel-cells. *J. Electroanal. Chem.* **357**, 201–224 (1993).
- [50] R. R. Chianelli, G. Berhault, B. Torres, Unsupported transition metal sulfide catalysts: 100 years of science and application, *Catalysis Today* **147**, 275–286 (2009).
- [51] J. G. Kushmerick, S. A. Kandel, P. Han, J. A. Johnson, and P. S. Weiss, Atomic-Scale Insights into Hydrodesulfurization, *J. Phys. Chem. B* **104**, 2980-2988 (2000).
- [52] X. Wang, H. Fang, Z. Zhao, A. Duan, C. Xu, Z. Chen, M. Zhang, P. Du, S. Song, P. Zheng and K. Chi, Effect of promoters on the HDS activity of alumina supported Co–Mo sulfide catalysts, *RSC Adv.* **5**, 99706-99711 (2015).
- [53] A.J.A.Konings, W. L. J Brentjens, D. C. K. Koninhsberger, and V. H. J. De Beer, ESR Studies on Hydrodesulfurization Catalysts: Nickel- or Cobalt-Promoted Sulfided Tungsten- or Molybdenum-Containing Catalysts, *Journal of Catalysis* **67**, 145-158 (1981).
- [54]. Baorui Xia, Qing Guo, Daqiang Gao, Shoupeng Shi and Kun Tao, High temperature ferromagnetism in Cu-doped MoS<sub>2</sub> nanosheets, *J. Phys. D: Appl. Phys.* **49** (2016) 165003
- [55]. Sohail Ahmed, Xiang Ding, Nina Bao, Pengju Bian, Rongkun Zheng, Yiren Wang, Peter Paul Murmu, John Vedamuthu Kennedy, Rong Liu, Haiming Fan, Kiyonori Suzuki, Jun Ding, and Jiabao Yi, Inducing High Coercivity in MoS<sub>2</sub> Nanosheets by Transition Element Doping, *Cite This: Chem. Mater.*, **29**, 9066-9074 (2017).
- [56]. S. S. Rao, K. N. Anuradha, S. Sarangi, and S. V. Bhat, Weakening of Charge Order and Anti Ferromagnetic to Ferromagnetic Switch Over in Pr<sub>0.5</sub>Ca<sub>0.5</sub>MnO<sub>3</sub> Nanowires, *Appl. Phys. Lett.*, **87**, 182503(2005).
- [57]. K.N. Anuradha, S. S. Rao and S.V.Bhat, Complete Melting of Charge Order in Hydrothermally Grown Pr<sub>0.57</sub>Ca<sub>0.41</sub> Ba<sub>0.02</sub>MnO<sub>3</sub> Nanowires, *Journal of nanoscience and nanotechnology*, **7**, 1775 (2007).
- [58]. Kinjal Gandha, Kevin Elkins, Narayan Poudyal, Xubo Liu & J. Ping Liu, High Energy Product Developed from Cobalt Nanowires, *SCIENTIFIC REPORTS* | 4 : 5345 | DOI: 10.1038/srep05345
- [59]. L. M. Martinez, M. D. Teran, R. R. Chianelli, S. R. J. Hennadige, S. R. Singamaneni, Magnetic Defects in Transitional Metal Di-Chalcogenide Semiconducting Layers, *MRS Advances*, DOI: 10.1557/adv.2018.110.

- [60]. L. M. Martinez, C. Karthik, M.R.Kongara, S. R. Singamaneni, Paramagnetic Defects in Hydrothermally Grown Few-Layered MoS<sub>2</sub> Nanocrystals, *Journal of Materials Research* **33**, 1656 (2018).
- [61]. Yanyu Wu, Maryam Zarei-Chaleshtori, Brenda Torres, Tahmina Akter, Carlos Diaz-Moreno, Geoffrey B. Saupe, Jorge A. Lopez, Russell R. Chianelli, Dino Villagran, Electrocatalytic hydrogen gas generation by cobalt molybdenum disulfide (CoMoS<sub>2</sub>) synthesized using alkyl-containing thiomolybdate precursors, *International journal of hydrogen energy* **42**, e20676 (2017).
- [62]. S. S. Rao, S. Narayana Jammalamadaka, A. Stesmans, V. V. Moshchalkov, J. van Tol, D. V. Kosynkin, A. Higginbotham and J. M. Tour, Ferromagnetism in Graphene Nanoribbons: Split Versus Oxidative Unzipped Ribbons, *Nano Letters* **12**, 1210 (2012).
- [63]. Jia Zhang, Jia Mei Soon, Kian Ping Loh, Jianhua Yin, Jun Ding, Michael B. Sullivan, and Ping Wu, Magnetic Molybdenum Disulfide Nanosheet Films, *Nano Letters* **7**, 2370 (2007).
- [64]. Xia, B., Yang, Y., Ma, J., Tao, K., Gao, D. Adjustable Ferromagnetic Behavior in Iron-Doped Two-Dimensional MoS<sub>2</sub> Multilayer Nanosheets. *Appl. Phys. Express*, **10**, 09332 (2017).
- [65]. Kanwal Preet Bhatti, Sujeet Chaudhary, Dinesh K. Pandya, and Subhash C. Kashyap, Intrinsic and extrinsic origin of room temperature ferromagnetism in ZnO:Co, *J. Appl. Phys.* **101**, 103919 (2007)
- [66]. Dezhi Wang, Xiangyong Zhang, Yilin Shen and Zhuangzhi Wu, Ni-doped MoS<sub>2</sub> nanoparticles as highly active hydrogen evolution electrocatalysts, Cite this: *RSC Adv.*, 2016, 6, 16656
- [67]. Sining Dong, Xinyu Liu, Xiang Li, Vasily Kanzyuba, Taehee Yoo, Sergei Rouvimov, Suresh Vishwanath, Huili G. Xing, Debdeep Jena, Margaret Dobrowolska, and Jacek K. Furdyna, Room temperature weak ferromagnetism in Sn<sub>1-x</sub>Mn<sub>x</sub>Se<sub>2</sub> 2D films grown by molecular beam epitaxy, *APL MATERIALS* **4**, 032601 (2016)
- [68] Chang-Soo Park, Dongil Chu, Yoon Shon, Juwon Lee, and Eun Kyu Kim, Room temperature ferromagnetic and ambipolar behaviors of MoS<sub>2</sub> doped by manganese oxide using an electrochemical method, *Appl. Phys. Lett.*, **110**, 222104 (2017)
- [69] H. Wang, C. Tsai, D. Kong, K. Chan, F. Abid-Pederson, J K. Nørskov, and Y Cui, Transition-metal doped edge sites in vertically aligned MoS<sub>2</sub> catalysts for enhanced hydrogen evolution, *Nano Research*, **8**, 566 (2015).
- [70] Dezhi Wang, Xiangyong Zhang, Yilin Shena, Zhuangzhi Wu, Ni-doped MoS<sub>2</sub> nanoparticles as highly active hydrogen evolution electrocatalysts *RSC Adv.*, **6**, 16656 (2016).
- [71] J. Deng, H. Li, J. Xiao, Y. Tu, D. Deng, H. Yang, H. Tian, J. Li, P. Ren, X. Bao, Triggering the electrocatalytic hydrogen evolution activity of the inert two-dimensional MoS<sub>2</sub> surface via single-atom metal doping, *Energy Environ. Sci.*, **8**, 1594-1601 (2015).

- [72] X. Ren, L. Pang, Y. Zhang, Xiaodong Ren, H. Fan, One-step hydrothermal synthesis of monolayer MoS<sub>2</sub> quantum dots for highly efficient electrocatalytic hydrogen evolution, *J. Mater. Chem. A*, **3**, 10693 (2015).
- [73] K. Ojha, S. Saha, S. Banerjee, A. K. Ganguli, Efficient Electrocatalytic Hydrogen Evolution from MoS<sub>2</sub>-Functionalized Mo<sub>2</sub>N Nanostructures. *ACS Appl. Mater. Interfaces*, **9**, 19455-19461 (2017).
- [74] X. Dai, K. Du, Z. Li, M. Liu, Y. Ma, H. Sun, X. Zhang, Co-Doped MoS<sub>2</sub> Nanosheets with the Dominant CoMoS Phase Coated on Carbon as an Excellent Electrocatalyst for Hydrogen Evolution, *ACS Appl. Mater. Interfaces*, **7**, 27242-27253 (2015).
- [75] Prins, R.; De Beer, V. H. J.; Somorjai, G. A., Structure and Function of the Catalyst and the Promoter in Co – Mo Hydrodesulfurization Catalysts, *Catalysis Reviews*, **31**, 1-41 (1989).
- [76] Z W Seh, J Kibsgaard, C F Dickens, Ib Chorkendorff, J K. Nørskov, T F. Jaramillo, Combining theory and experiment in electrocatalysis: Insights into materials design, *Science* **355**, 146 (2017) DOI: 10.1126/science.aad4998
- [77]. D Merki, H Vrubel, L Rovelli, Stéphane Fierro and Xile Hu Fe, Co, and Ni ions promote the catalytic activity of amorphous molybdenum sulfide films for hydrogen evolution, *Chem. Sci.*, **3**, 2515-2525 (2012).
- [78]. P. W. Selwood, Magnetism and Catalysis, *Chem. Rev.*, **38**, 41–82 (1946).
- [79]. James T. Richardson, Magnetism and catalysis, Citation: *J. Appl. Phys.*, **49**, 1781 (1978); doi: 10.1063/1.324865.
- [80] R. J. H. Voorhoeve, Experimental Relationships between Catalysis and Magnetism, *AIP Conference Proceedings* **18**, 19 (1974).
- [81]. Torun, E., Fang, C. M., de Wijs, G. A. & de Groot, R. A. Role of Magnetism in Catalysis: RuO<sub>2</sub> (110) Surface, *Journal of Physical Chemistry C*. **117**, 6353-6357 (2013).